Chimera state in complex networks of bistable Hodgkin-Huxley neurons

A. V. Andreev,[1] N. S. Frolov,[1] A. N. Pisarchik,[2,1] and A. E. Hramov[1,3,*]

[1]*Neuroscience and Cognitive Technology Laboratory, Center for Technologies in Robotics and Mechatronics Components, Innopolis University, Universitetskaya, 1, Innopolis, Republic of Tatarstan, 420500, Russia*

[2]*Center for Biomedical Technology, Technical University of Madrid, Campus Montegancedo, 28223 Madrid, Spain*

[3]*Saratov State Medical University, Bolshaya Kazachia st., 112, Saratov, 410012, Russia*

(Received 23 June 2019; published 30 August 2019)

In this paper we study a chimera state in complex networks of bistable Hodgkin-Huxley neurons with excitatory coupling, which manifests as a termination of spiking activity of a part of interacting neurons. We provide a detailed investigation of this phenomenon in scale-free, small-world, and random networks and show that the chimera state is robust to the network topology. Nevertheless, network topological properties determine the stability of spatiotemporal states and therefore affect the excitability of the chimera state in the whole network. In particular, the scale-free network whose higher degree nodes are more stable to small perturbations is least exposed to chimera formation and exhibits an abrupt transition from a spiking to a silent regime. On the other hand, small-world and random networks are more likely to provide transitions to the chimera state.

DOI: 10.1103/PhysRevE.100.022224

I. INTRODUCTION

A brain neuronal network composed of a large number of interconnected neurons is one of the most complex self-organized systems in nature [1–3]. Understanding brain functionality, i.e., how this complex biological system works, through computer simulations of neural cooperation dynamics is one of the fundamental challenges of modern science. Modern theories state that self-organized neuronal populations provide mechanisms for normal brain functioning, i.e., synchronous firing in local neuronal groups and interareal communication through coherence of brain rhythms [4–9].

Although self-organization in neuronal ensembles has received much attention in recent years, many phenomena still remain poorly studied. Furthermore, a variety of new unexpected effects have been discovered. For a long time it has been believed that a network of interconnected elements can exhibit either completely synchronous or asynchronous behaviors. At this point, a chimera state, manifesting the coexistence of synchronous and asynchronous subgroups within an entire ensemble [10,11], is a fascinating type of the collective effect which reflects real-life behavior of physical [12–16], ecological [17–19], and even social systems [20]. Chimera states are usually believed to be chaotic transients, which eventually collapse to a synchronized state [21,22]. For example, Banerjee and Sikder [23] demonstrated that small chimeras in the local flux dynamics of an array of magnetically coupled superconducting quantum interference devices (SQUIDs) driven by an external field are born through transient chaos.

Chimera states in neuronal systems were extensively studied due to their promising applications in neuroscience (see the comprehensive review of Majhi *et al.* [24]). In particular, the chimera state could be relevant to bump states in neural systems [25] and a multitude of neuronal disorders, including Alzheimer's and Parkinson's diseases, epilepsy, brain tumors, etc. [26–28]. Despite the lack of experimental verification of chimera states in neuronal systems due to their extraordinary complexity [29], this phenomenon has been widely analyzed in networks of simplified Hodgkin-Huxley neurons, namely, FitzHugh-Nagumo and Hindmarsh-Rose models. For instance, Bandyopadhyay and Kar [30] studied synchronization in networks of Hindmarsh-Rose neurons of random, regular, small-world, scale-free, and modular topologies. They demonstrated the emergence of chimera-like states in some small-world and modular networks.

For the last few years a number of remarkable fundamental effects have been uncovered in model neuronal networks. Recent papers report a multitude of chimera patterns in multiplex networks [31–34]. For example, a link between coherence resonance and a chimera state was found in a network of excitable units [35,36]. Chimera states were also observed in empirical brain networks, namely, in the *C. elegans* soil worm connectome [37], cats [38], and healthy humans using diffusion-weighted magnetic resonance imaging (MRI) data [39]. Recently, special interest has been paid to revealing chimera states in neuronal hypernetworks and networks of networks [40,41]. In this context, the analysis of model neuronal networks remains a challenging task since the discovery of the existence of a number of new intriguing nontrivial effects that deserve careful consideration.

The coexistence of different brain states is another important issue that should also be taken into account while studying neuron dynamics [42]. Switches between such coexisting states play an important role in cell signaling and neuronal interactions [43–45]. Typically, each cell receives inputs from thousands of cells mediated by many different neurotransmitters and consequently modifying the postsynaptic potential by excitation or inhibition [46]. Communication between cells takes place at synaptic contacts, where an arriving action potential releases a neurotransmitter, thus affecting the

*a.hramov@innopolis.ru

postsynaptic potential of the target cell. It is believed [47] that the coexisting dynamical regimes mimic different brain states representing particular objects of perception which can be selected by giving the neural network an input corresponding to an initial condition [48–50]. Furthermore, the coexistence of multiple states in the brain has been proposed as a basic mechanism for associative content-addressable memory storage and pattern recognition in neural systems [47,51–53].

Collective dynamics in a neuronal network is usually considered by supposing that every neuron in the network is monostable. However, according to Keener and Sneyd [54], the Hodgkin-Huxley (HH) model exhibits bistability in a narrow range of control parameters near the excitation threshold. The bistability regime in oscillatory systems is known to be of special interest due to a variety of hidden unexpected phenomena. In particular, Nekorkin *et al.* [55,56] found theoretically and experimentally both amplitude and phase chimeras in the network of electronic oscillators constructed on the base of a generic self-excited bistable model. Concerning neuronal models, it is worth mentioning the recent work of Uzuntarla *et al.* [57], who uncovered a counterintuitive effect in the neuronal network of bistable HH neurons, where a spiking behavior transformed into a steady state under excitatory coupling. We suppose the origin of this lies in the coexistence of spiking and silent neural populations in the neuronal network, which can be referred to as a chimera state. Such kind of chimeras may shed light on the unihemispheric brain slow-wave sleep in mammalians and birds [58,59]. The dynamics of the network of bistable HH neurons was recently studied by Esir *et al.* [60], who highlighted the role of coupling delays and noise in formation of up and down states in the neuronal network.

In this paper we carry out a detailed numerical analysis of the chimera state in complex networks of coupled bistable excitatory HH neurons with coexistence of spiking and silent neuronal subgroups. We focus on the inference of physical mechanisms responsible for annihilation of the spiking behavior under neural interaction, and reveal conditions for a specific type of chimeras in the network of HH neurons. As distinct from the work of Esir *et al.* [60], where switches between coexisting states were induced by noise, in our model the chimera state appears in a completely deterministic system. Considering different network topologies, scale-free, small-world, and random, we demonstrate, for the first time to the best of our knowledge, the robustness of the observed chimera patterns to structural properties of the network. We show that topology plays an important role in stability of individual nodes and, therefore, affects the chimera state excitability in the whole network.

The paper is organized as follows. In Sec. II we describe the numerical model and consider individual dynamics of a bistable HH neuron with two coexisting attractors (fixed point and limit cycle). We also demonstrate features of the switching behavior between these attractors due to a short-pulsed external current which changes neuron dynamics from a silent to a spiking regime and vise versa. Then in Sec. III we analyze the collective neuronal behavior and reveal regions of the chimera state in scale-free, small-world, and random HH neuronal networks. In Sec. IV we discuss the problem of nodes stability with respect to different network topology and draw conclusions about the influence of structural properties on transitions between various regimes of the collective behavior. Finally, the results are summarized in Sec. V.

II. DYNAMICS OF A SINGLE BISTABLE HODGKIN-HUXLEY NEURON

Let us start with consideration of a bistable HH neuron. Temporal evolution of the membrane potential and gating variables of the HH neuron can be described by the following differential equations [61]:

$$C_m\frac{dV}{dt} = -g_{Na}^{\max}m^3h(V-V_{Na}) - g_K^{\max}n^4(V-V_K) - g_L^{\max}(V-V_L) + I^e, \tag{1}$$

$$\frac{dx}{dt} = \alpha_x(V)(1-x) - \beta_x(V)x, \qquad x = m, n, h, \tag{2}$$

where $C_m = 1\ \mu\mathrm{F/cm}^3$ is the capacity of the cell membrane, I^e is the external bias current (in $\mu\ \mathrm{A/cm}^2$), V is the membrane potential (in mV), $g_{Na}^{\max} = 120\ \mathrm{mS/cm}^2$, $g_K^{\max} = 36\ \mathrm{mS/cm}^2$, and $g_L^{\max} = 0.3\ \mathrm{mS/cm}^2$ are maximal sodium, potassium, and leakage conductances, respectively, when all ion channels are open, $V_{Na} = 115$ mV, $V_K = -12$ mV, and $V_L = -10.6$ mV are reversal potentials for sodium, potassium, and leak channels, respectively, m, n, and h represent mean ratios of open gates of specific ion channels, n^4 and m^3h are mean portions of open potassium and sodium ion channels within a membrane patch, and $\alpha_x(V)$ and $\beta_x(V)$ are rate functions given as [62]

$$\alpha_m(V) = \frac{0.1(25-V)}{\exp[(25-V)/10]-1}, \tag{3}$$

$$\beta_m(V) = 4\exp(-V/18), \tag{4}$$

$$\alpha_h(V) = 0.07\exp(-V/20), \tag{5}$$

$$\beta_h(V) = \frac{1}{1+\exp[(30-V)/10]}, \tag{6}$$

$$\alpha_n(V) = \frac{0.01(10-V)}{\exp[(10-V)/10]-1}, \tag{7}$$

$$\beta_n(V) = 0.125\exp(-V/80). \tag{8}$$

The numerical calculations of Eq. (1)–(8) were performed using the fourth-order Runge-Kutta algorithm with a fixed integration time step $\Delta t = 10\ \mu$s.

The external current I^e controls the neuron dynamics. Depending on its value, the HH neuron can be either in a silent (fixed point) or a spiking (limit cycle) regime. Keener and Sneyd [54] demonstrated the existence of bistability within a narrow range of I^e where these two attractors coexist. In Fig. 1 this region is highlighted in gray. For $I^e < 6.24\ \mu\mathrm{A/cm}^2$ only a stable fixed point (FP) exists, whereas for $I^e \geqslant 9.78\ \mu\mathrm{A/cm}^2$ there is only a stable limit cycle (LC). So a tipping point occurs at $I^e = 6.24\ \mu\mathrm{A/cm}^2$ where the neuron generates spikes at certain initial conditions. According to Ref. [54] a further increase in the external current results in the transition to the fixed point through a Hopf bifurcation. Since we are interested in bistable HH dynamics, we

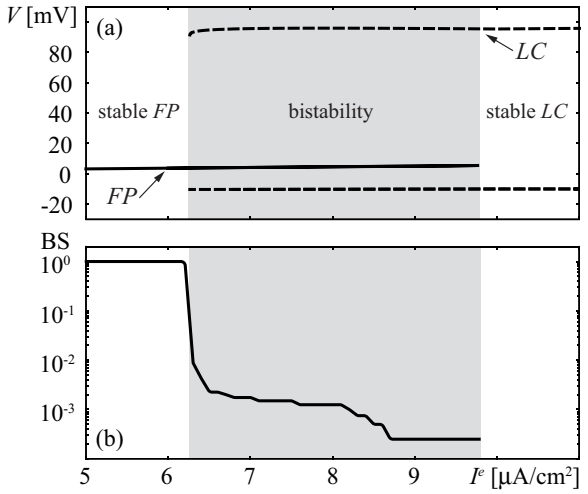

FIG. 1. (a) Bifurcation diagram of a single HH neuron with external current I^e as a control parameter. Here FP and LC indicate a fixed point and a limit cycle, respectively. (b) Basin stability of the FP attractor. The gray area indicates the bistability region with coexisting fixed point (solid line) and limit cycle (dotted line).

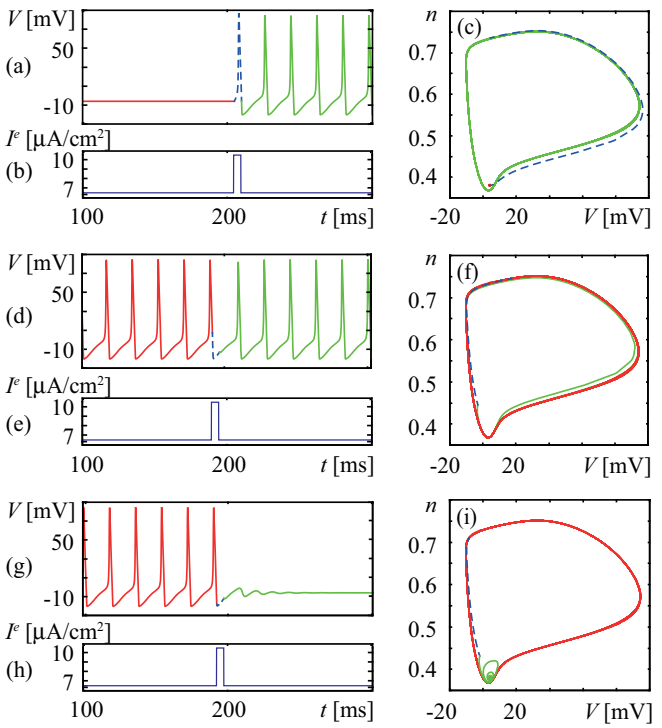

FIG. 2. (Left column) Time series of membrane potential V of a single HH neuron and short-pulsed external current I^e and (right column) phase portraits on the (V, n) plane. (a)–(c) Switching from a fixed point to a limit cycle. (d)–(f) Conserving a limit cycle when the external pulse is introduced at an improper phase ($t_0 = 191.5$ ms). (g)–(i) Switching from a limit cycle to a fixed point ($t_0 = 192$ ms). Dark gray (red online), dotted gray (blue online), and solid gray (green online) highlight neuron stages before, during, and after the pulse application, respectively.

restrict our consideration on the bistability range $6.24 \leqslant I^e < 9.78\ \mu\text{A/cm}^2$.

It is important to note that a relative volume of the basin of attraction of the FP attractor estimated via the basin stability (BS) analysis [63,64] abruptly reduces as the external current is increased after passing the tipping point at $I^e = 6.24\ \mu\text{A/cm}^2$ [see Fig. 1(b)]. To perform the BS analysis, we integrated Eqs. (1)–(8) for $t = 2$ s $M = 4000$ times, every time starting from a random initial condition. The FP size was estimated as the ratio $BS_{FP} = M_{FP}/M$, where M_{FP} is the number of trajectories terminated at the FP attractor.

Despite the basin of attraction of the FP state is very small, switches between FP and LC states are possible if the value of the external current I^e is suddenly increased. Let us now consider the dynamics of a single HH neuron perturbed by a short perturbation $\widetilde{I}^e(t)$ of the external current modeled by a boxcar function as

$$\widetilde{I}^e(t) = I^e + I_0^e[H(t - t_0) - H(t - t_0 - \Delta t)], \qquad (9)$$

where I_0^e is the amplitude of the external current perturbation, $H(\bullet)$ is the Heaviside step-function, t_0 is the moment of time when the perturbation is applied, and Δt is the short external current pulse.

The effect of the external current perturbation is illustrated in Fig. 2. The following parameter values were chosen. The constant external current was fixed at $I^e = 6.5\ \mu\text{A/cm}^2$ that led to the basin size $BS_{FP} \approx 2 \times 10^{-3}$, the pulse duration was $\Delta t = 5$ ms, and the pulse amplitude was $I_0^e = 4\ \mu\text{A/cm}^2$.

The chosen values of the amplitude and pulse duration are comparable with that of a single neuron during its interaction with other neurons in the network. The switches from a fixed point to a limit cycle [Fig. 2(a)–2(c)] do not require a high pulse amplitude because the basin of attraction of the limit cycle is much larger than the basin size of the FP. Therefore, a relatively small perturbation of the external current can provide the neuron leaving the FP basin of attraction. In turn, the inverse transition, i.e., from a limit cycle to a fixed point [Figs. 2(g)–2(i)], is much more sensitive to the pulse parameters, especially to the moment of time t_0 when the external pulse is applied. For instance, if the perturbation is applied at an inappropriate phase of the limit cycle trajectory, when it passes far from the FP basin of attraction, the attractor will not change [Figs. 2(d)–2(f)]. After a slight trajectory deviation the neuron returns back to the limit cycle attractor and continues spiking. On the other hand, if the neuron dynamics is disturbed at the correct phase when the phase trajectory passes close to the FP, the perturbation of the external current switches the neuron state to the FP [Figs. 2(g)–2(i)]. It should be noted that the difference between a correct and a wrong phase for switching is very small and equal to approximately 0.5 ms because the FP is located very close to the limit cycle in the phase space. Therefore, the switching from the limit cycle to FP is possible only within a narrow time window during the oscillation period.

III. COLLECTIVE BEHAVIOR IN A HODGKIN-HUXLEY NEURONAL NETWORK

In this section we study collective dynamics of a neuronal network composed of $N = 100$ HH bistable neurons. To

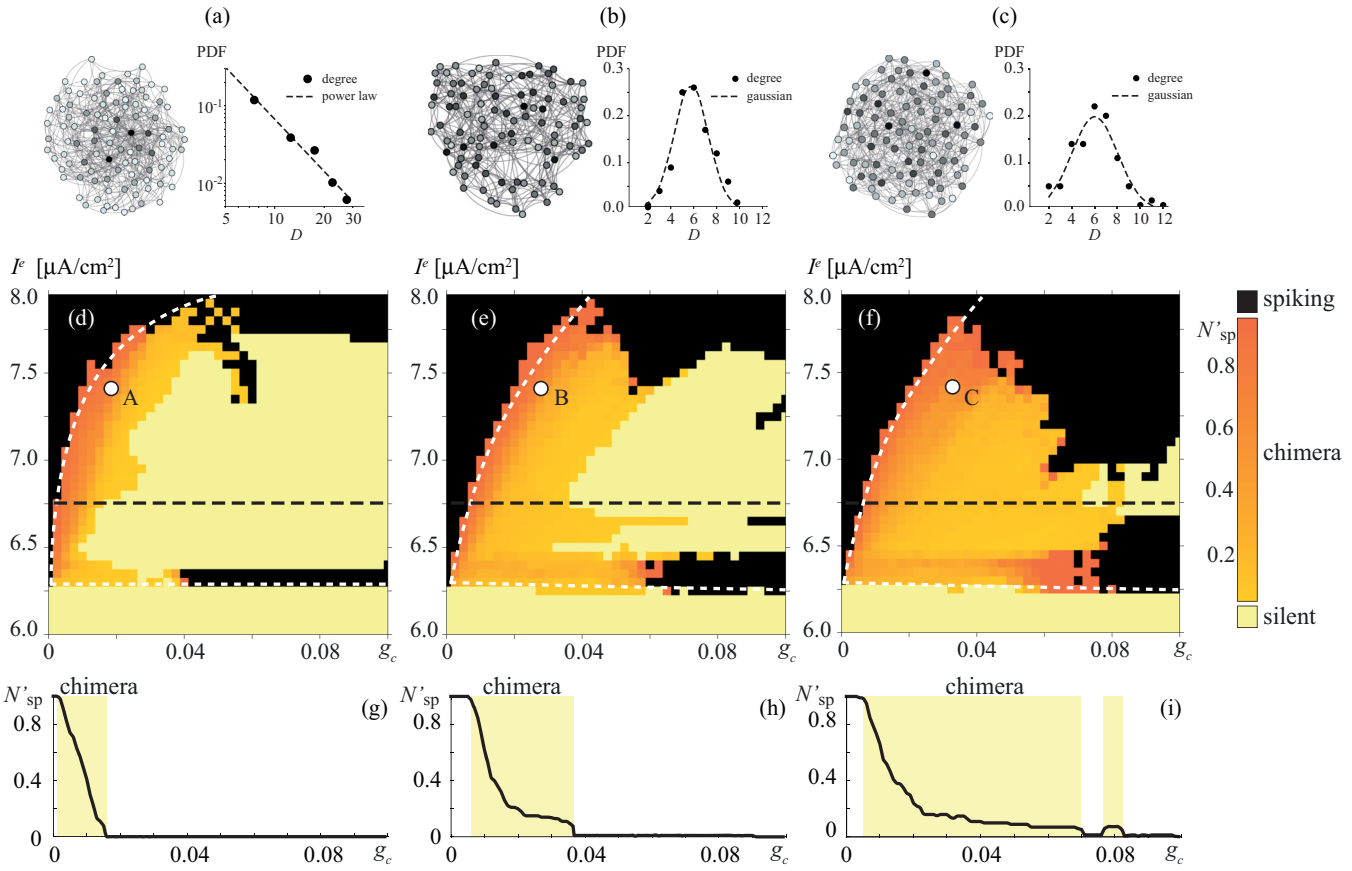

FIG. 3. Emergence of partially spiking chimera states in neuronal networks of different topologies. (a)–(c) Scale-free, small-world, and random network topologies (left panels) and corresponding degree D probability density functions (PDFs) (right panels). Black, gray, and empty dots in the networks indicate nodes with high, medium, and low degree, respectively. The dashed lines and points in the PDF plots show theoretical and empirical dependencies, respectively. (d)–(f) Relative number of spiking neurons (N'_{sp}) in the two-parametric space of coupling strength g_c and external current I^e. Dashed lines indicate the boundaries between different types of collective dynamics: Silent [light gray (yellow online)], spiking (black) and chimera [gray (orange online)]. (g)–(i) Relative number of spiking neurons (N'_{sp}) versus g_c at $I^e = 6.75$ [sections of the maps in panels (d)–(f) shown by large-dashed horizontal lines]. Network dynamics at points A, B, and C are illustrated in Fig. 4.

model network interactions we introduce chemical synaptic coupling so that Eqs. (1) and (2) take the following form:

$$C_m \frac{dV_i}{dt} = -g_{Na}^{\max} m_i^3 h_i (V_i - V_{Na}) - g_K^{\max} n_i^4 (V_i - V_K) - g_L^{\max} (V_i - V_L) + I^e + I_i^{\text{syn}}, \tag{10}$$

$$\frac{dx_i}{dt} = \alpha_{x_i}(V_i)(1 - x_i) - \beta_{x_i}(V_i) x_i, \quad x = m, n, h, \tag{11}$$

where I_i^{syn} is the total synaptic current received by the ith neuron. Following Ref. [65] the synaptic current is given as

$$I_i^{\text{syn}} = \sum_{j \in M_i} g_c \alpha(t - t_0^j)(E_{rev} - V_i), \tag{12}$$

where g_c is the maximal conductance of a synaptic channel in mS/cm^2 referred to as a coupling strength, M_i is the set of indices of the neurons coupled with the ith neuron, defined by the adjacency matrix, and t_0^j is the moment of time when the jth (presynaptic) neuron fires. Here the temporal evolution of synaptic conductance is described as

$$\alpha(t) = e^{-t/\tau_{\text{syn}}} H(t), \tag{13}$$

where $H(\bullet)$ is the Heaviside step function and $\tau_{\text{syn}} = 3$ ms.

Now we consider how the network topology affects collective dynamics of the coupled bistable HH neurons. The networks of three different topologies, scale-free (SF), small-world (SW), and random, are schematically illustrated in the left panels of Figs. 3(a), 3(b), and 3(c), respectively. In real neuronal ensembles, the SW property determines neuronal coupling on an anatomical level [2,66], whereas the SF topology is inherent in functional brain networks and determines the interaction between distinct brain regions through low-frequency oscillatory coherence [3,67]. The adjacency matrix for the SF network is generated using the Barabási-Albert algorithm [68], which creates a graph of $N = 100$ nodes having $m = 5$ edges each. Whereas, the SW network is generated using the Watts-Strogatz model [69] with parameters $\beta = 0.3$ and $K = 5$. The parameter β is the probability for a particular link in the initially regular topology to be randomly rewired, and K is the mean degree. The completely random network is generated as a limit case of the Watts-Strogatz model with

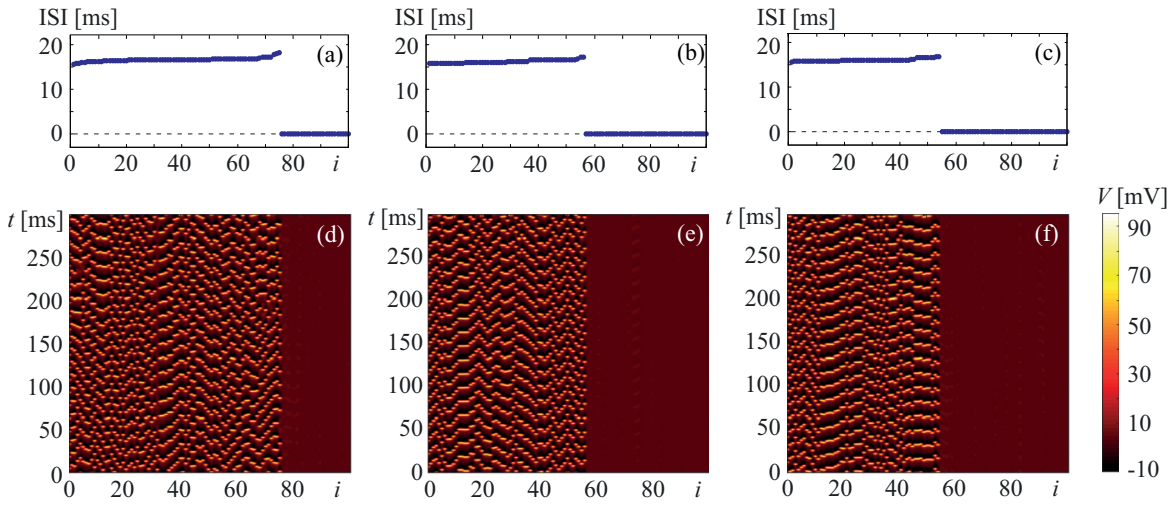

FIG. 4. Illustration of partially spiking chimera patterns in different types of HH neuronal networks. (a)–(c) Distribution of averaged interspike interval (ISI) over the network and (d)–(f) spatiotemporal patterns for different network topologies: (a), (d) scale-free ($g_c = 0.0175$ mS/cm^2, point A in Fig. 3), (b), (e) small-world ($g_c = 0.0275$ mS/cm^2, point B in Fig. 3), and (c), (f) random ($g_c = 0.0325$ mS/cm^2, point C in Fig. 3). The external current is fixed at $I^e = 7.4$ μA/cm^2.

$\beta = 1$, meaning that all links of the initially regular topology are randomly rewired.

Next, we analyze the network dynamics with respect to two control parameters, external current I^e and maximal conductance of synaptic channel g_c. While the former determines individual dynamics of each HH neuron, the latter controls collective dynamics of the whole network, i.e., the coexistence of silent and spiking neuron ensembles. Let us first quantify the state of the neuronal network as the relative number of spiking neurons $N'_{sp} = N_{sp}/N$, where N_{sp} is the absolute number of spiking neurons in the network. Figures 3(d), 3(e), and 3(f) show the distributions of N'_{sp} in the (g_c, I^e) parametric space for SF, SW and random networks, respectively. As we have shown in Sec. II, $I^e = 6.24$ μA/cm^2 is a threshold value of the external current, below which only a stable steady state exists in a single HH neuron. Obviously, below the threshold the same silent behavior also occurs in the neuronal network regardless of the network topology. In Figs. 3(d)–3(f) this threshold is marked by the dashed horizontal line. One can see that below this line all neurons are in the silent regime, i.e., $N'_{sp} = 0$ for any g_c. However, if the external current exceeds the threshold ($I^e > 6.24$ μA/cm^2), transitions between "all spiking" (purple area) and "all silent" (yellow area) states occur in the neuronal networks for particular values of the control parameters.

Evidently, an increase in g_c results in a growth of the synaptic current $I_i^{\rm syn}$ which plays the same role as the short external pulse applied to a single neuron (see Sec. II). According to the above discussion of single HH neuron dynamics, feeding a neuron with a synaptic current pulse via excitatory coupling with its neighbors can terminate its spiking. Also, the larger the $I_i^{\rm syn}$ amplitude, the higher the probability of switching the neuron to a silent state. Interestingly, the transition "all spiking" $\rightarrow$ "all silent" does not happen abruptly, but is followed by the emergence of an intermediate state with coexisting spiking and silent neuronal subpopulations, which we refer to as a specific type of chimera in the network of bistable neurons.

It is worth mentioning that similar chimeras of bistable elements were previously described in other papers [16,70,71]. In particular, Shchapin *et al.* [55] found amplitude and phase chimeras both theoretically and experimentally in the network of electronic oscillators constructed on the base of a generic self-excited bistable model. They observed that the network of bistable elements splits into two subnetworks with different dynamics. This new state was referred to as a chimera state.

As seen from Figs. 3(d)–3(f) the appearance of the chimera state in the network of bistable neurons is a universal effect regardless of the network topology. Nevertheless, structural properties of neuronal networks strongly affect the size of the chimera patterns in the parametric space. In particular, the smallest chimera region is observed in the SF network, whereas the largest region occurs in the random network. Moreover, a decrease of the spiking neuron population under a growth of g_c is rather smooth in the random and SW networks [Figs. 3(h) and 3(i)]. Instead, the transition to a silent regime in the SF network is very sharp [Fig. 3(g)]. According to Scheffer *et al.* [72], networks with a low level of connectivity, like completely random or SW networks [see degree distributions in Figs. 3(b) and 3(c)], are gradually adjusted to the variation of control parameters, resulting in a smooth change of their global state. Thus, partially spiking chimera states, intermediate states between globally spiking and globally silent behavior, are more pronounced in such networks.

On the other hand, the highly connected SF network [see degree distribution in Fig. 3(a)] responds to changes in control parameter in the form of critical transitions. In this network, small perturbations of globally coherent states are repaired by the inputs from linked neighboring units, so that qualitative changes in the network dynamics occur abruptly in the vicinity of a critical point. This explains a relatively small size of

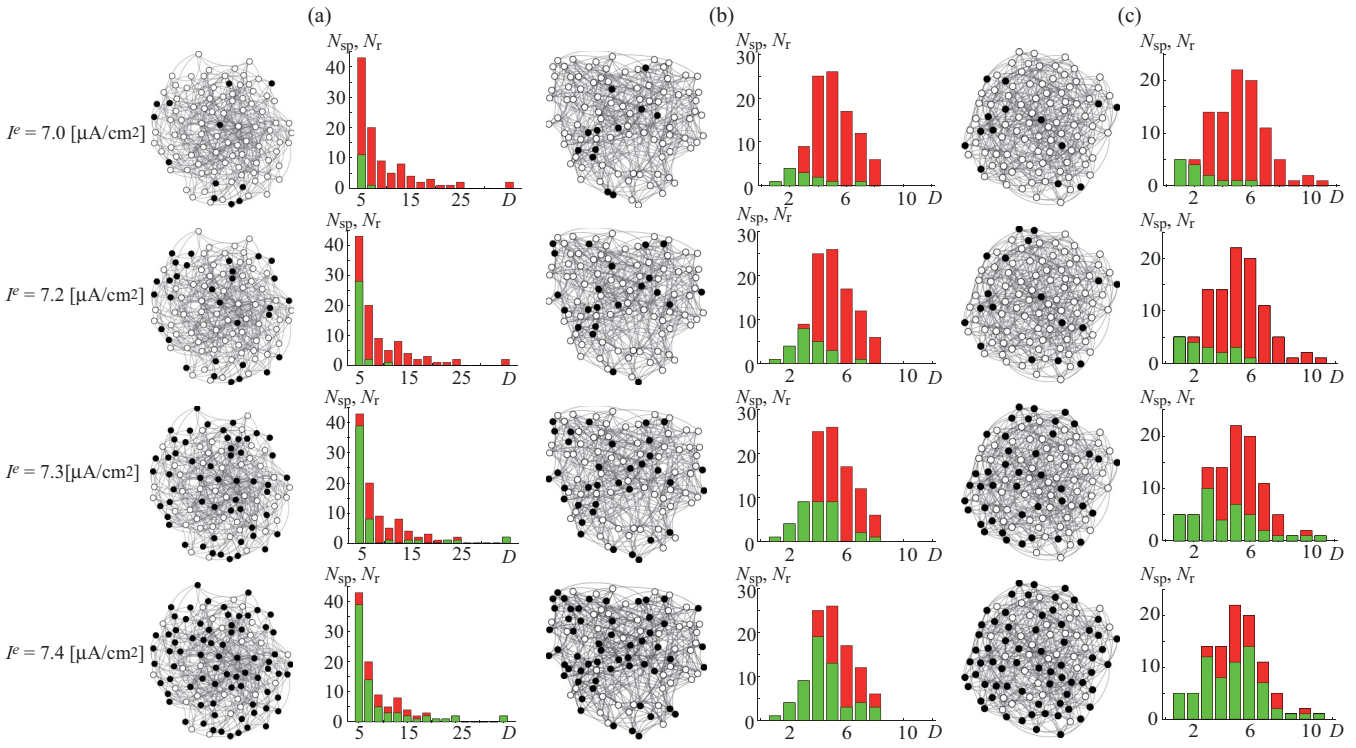

FIG. 5. Distribution of silent (empty dots) and spiking (closed dots) in (a) scale-free, (b) small-world, and (c) random neuronal networks under variation of external current I^e. (Left-side columns) Network topologies and (right-side columns) distributions of the number of spiking [N_{sp}, gray (green online)] and silent [N_r, dark gray (red online)] neurons. Each row corresponds to different value of external current I^e indicated at the left side. Maximal conductances fixed for different network topologies are $g_c = 0.0175$ mS/cm^2, $g_c = 0.0275$ mS/cm^2, and $g_c = 0.0375$ mS/cm^2 for SF, SW, and random network, respectively.

the chimera region in the SF network as compared to SW and random networks. Importantly, the number of spiking neurons in the chimera region changes smoothly with respect to the control parameters, regardless of the network topology. This gives the possibility to control the size of the spiking area by changing the control parameters.

Typical chimera patterns in neuronal networks of different topologies are illustrated in Fig. 4. These states correspond to the parameter values at points A, B, and C in Fig. 3. For better visualization we sorted the network elements according to the average interspike interval (ISI) presented in Figs. 4(a)–4(c). Here ISI = 0 characterizes silent neurons. As seen from Figs. 4(d)–4(f), at certain conditions all networks self-organize to form pronounced chimera patterns of coexisting silent and phase-locked spiking neuron populations.

Let us now consider the process of the coherent pattern formation under increasing external current I^e from the viewpoint of the network topological properties. In the left columns of Figs. 5(a)–5(c) we plot the neuron populations of spiking (closed dots) and silent (open dots) elements for different values of the external current I^e and fixed maximal conductance g_c for each network topology (Fig. 3). One can see that once the neurons are activated, they continue spiking with increasing I^e (from up to down in Fig. 3), involving more and more neurons into the spiking regime. Obviously, such a behavior is affected by the network structure. In other words, the probability of an individual node to be activated is closely related to its degree. The right columns in Figs. 5(a)–5(c) evidence the fact that nodes with lower degree are more likely to be switched from silent to spiking activity as I^e is increased. This happens because a low-degree node poorly interacts with other network elements and does not have enough subsidiary inputs to be "repaired," i.e., to turn back to the less stable FP attractor. By contrast, a high-degree node is strongly affected by the excitatory coupling summarized over many network nodes, which makes the FP (silent state) more stable and decreases the probability of this node to be switched to a limit cycle (spiking regime).

The uncovered property is universal with respect to network topology. Moreover, it provides insight into the relation between the size of the chimera region and the network topology. One can see that the SF network is characterized by a large number of low-degree nodes that determine a rapid growth of the spiking neuron population and, therefore, a fast transition from a globally silent to a globally spiking regime and vice versa. In turn, the SW and random networks have a pronounced distribution of the node degrees that provide a smooth growth of the spiking subgroup.

IV. NODE STABILITY IN THE BISTABLE HODGKIN-HUXLEY NETWORK

Now we address the issue of excitability of the partially spiking chimera pattern under a short external current pulse applied to the entire network. As was shown in Sec. II, the pulse induces a transition of a single neuron from a resting to a spiking state and vice versa. So we expect that a small

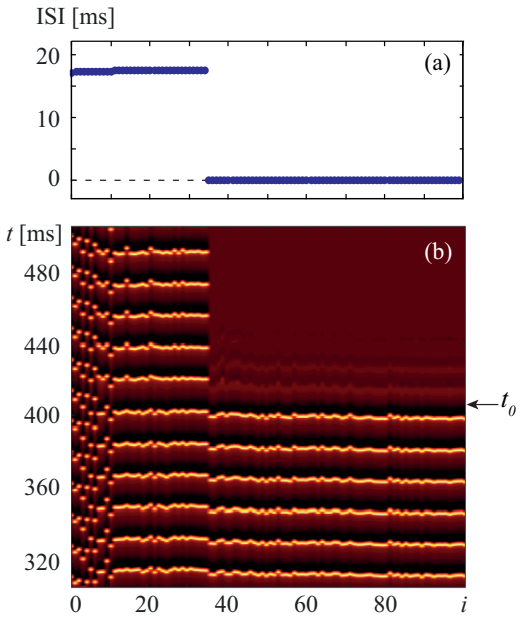

FIG. 6. Partial termination of spiking activity in a scale-free network of bistable HH neurons under small perturbation of external current $\widetilde{I}^e$. (a) Interspike intervals distribution averaged over a 100-ms time interval after the external pulse was applied. (b) Spatiotemporal dynamics under the influence of the external current pulse. The arrow indicates the moment of time t_0 when the pulse is applied.

perturbation of a totally spiking neuronal network will cause a partial or a complete termination of the spiking behavior.

By analogy with Sec. III, we apply a short ($\Delta t = 5$ ms) pulse to the external current at $t_0 = 405$ ms in the form of a boxcar function given by Eq. (9). To test the network stability, we introduce the small deviation of the external current $I_0^e = 0.5\ \mu\text{A/cm}^2$ to the totally spiking neuronal network in the vicinity of the chimera boundary, with the following control parameters: $I^e = 7\ \mu\text{A/cm}^2$ and $g_c = 0.0025\ \text{mS/cm}^2$. Figure 6(a) illustrates the evolution of the SF network under the external perturbation. One can see that some of the spiking neurons ($i \leqslant 35$) are robust to the external perturbation and remain in the spiking mode, while other neurons ($i \geqslant 36$) switch to a silent regime. Similar to a single HH neuron, the entire neuronal network is also sensitive to the moment of time (or phase) when the external perturbation is applied.

In Fig. 7 we plot the spiking neuron population size as a function of time t_0 when the external perturbation is applied. One can see that this dependence has a pronounced minimum regardless of the network type, corresponding to the phase of periodic trajectory optimal for switching the most of the neurons to the silent state.

In this context, it is also interesting to reveal stability properties of network nodes with respect to their degree. With this goal we consider 20 randomly generated networks for each type of network topology, sort their elements according to their node degree, and perturb them as described above. Afterwards, we compare the average degree D of ith node with its probability $s_i = M_{sp}^i/20$ (M_{sp}^i being the number of times the ith node continue spiking) to maintain the spiking

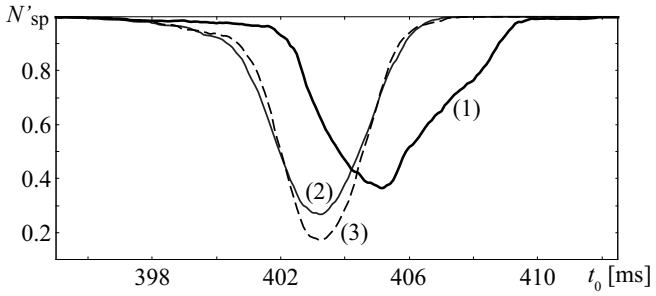

FIG. 7. Relative size of spiking neuron population N_{sp}/N versus time t_0 of the short pulse introduction during one spiking period for (1) scale-free, (2) random, and (3) small-world networks. Each curve is averaged over the set of 20 randomly chosen networks of the corresponding type.

behavior and find a very good correlation. Therefore, we conclude that the nodes with higher degree are likely to maintain the spiking regime (see Fig. 8). This property is highly manifested in the SF network of bistable HH neurons due to the presence of nodes with extremely high degree [Figs. 8(a) and 8(d)]. By contrast, in the SW and random networks the variation of the node degree distribution is not well pronounced, thus resulting in a homogeneous distribution of probability s [Figs. 8(c)–8(f)].

V. CONCLUSION

In this paper we have studied a phenomenon of partially spiking chimera behavior induced in complex networks of bistable Hodgkin-Huxley neurons with excitatory coupling. Our finding evidences a counterintuitive phenomenon that an increase in the excitatory coupling strength leads to the termination of a globally spiking behavior of a neuronal network. This is possible due to specific dynamical features of a single bistable HH neuron, where an external current pulse leads to switches between coexisting attractors, i.e., from a fixed point (silent state) to a limit cycle (spiking state) and vice versa. Moreover, the probability of the "limit cycle" → "fixed point" transition is proportional to the external pulse parameters. Specifically, a strong interaction between network elements stabilizes the silent state in the network. In contrast to Banerjee and Sikder [23], who observed the emergence of small chimera states out of transient chaos in the model of nonlinear metamaterial, in our model the chimera is born as a result of bistability in the individual network element.

Here we have demonstrated that along with globally spiking and globally silent dynamics, complex neuronal networks exhibit a specific type of a collective behavior manifesting as a long-term stable coexistence of spiking and silent ensembles. Having considered scale-free, small-world, and completely random networks, we have shown that a partially spiking chimera pattern is a universal phenomenon which emerges regardless of the network topology. However, the network structural properties strongly affect the size of the chimera region in the parameter space. According to our results of the extensive computational studies, highly connected networks, e.g., scale-free, are characterized by a narrow region of the chimera behavior, by contrast with networks with lower

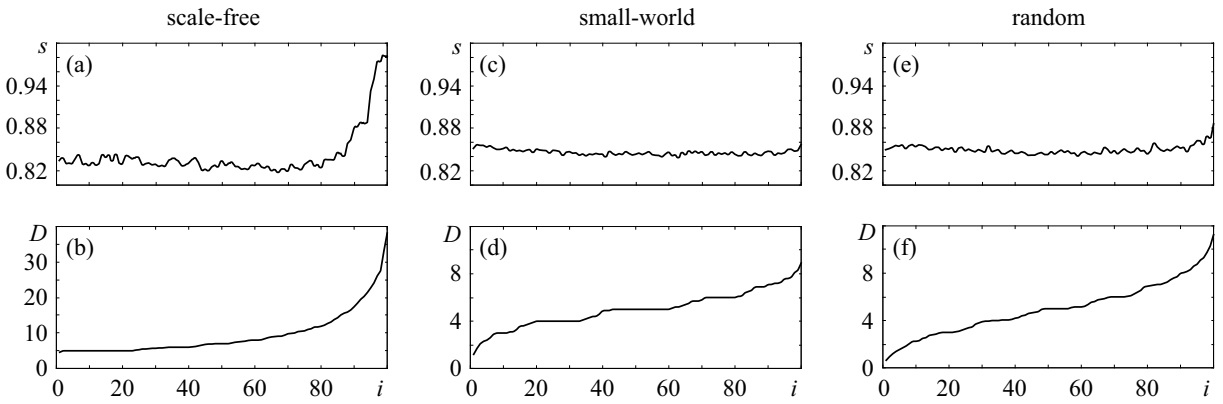

FIG. 8. Relation between node stability and its degree D. (a)–(c) Probability of a node to maintain the spiking regime and (d)–(f) node degree distribution. Each plot is an average over 20 different realizations in networks of the same topology: (a), (d) scale-free, (b), (e) small-world, and (c), (f) random.

connectivity, like small-world and random, where chimera states are observed in a considerably wider area. As distinct from the work of Bandyopadhyay and Kar [30], who found chimera-like states in small-world and modular networks of Hindmarsh-Rose neurons, we have demonstrated the emergence of chimera states not only in small-world but also in scale-free and completely random networks of Hodgkin-Huxley neurons.

We have also demonstrated the possibility to control the size of the spiking neuron population by applying a short external current pulse. In this context, structural properties play a crucial role in stability of nodes with respect to small perturbations of a control parameter. In particular, we have found a negative correlation between node degree and its probability to switch to a silent state under the external pulse. We believe that apart from fundamental interest to provide new insight into neuronal interactions, the uncovered chimera state may also have potential applications for the development of pulsed signal classifiers based on interconnected biological neurons.

ACKNOWLEDGMENTS

This work has been supported by the Russian Science Foundation (Grant No. 17-72-30003). A.N.P. acknowledges support from the Spanish Ministry of Economy and Competitiveness under project SAF2016-80240 for the method development.

[1] O. Sporns, Dialogues Clin. Neurosci. **15**, 247 (2013).
[2] S. F. Muldoon, E. W. Bridgeford, and D. S. Bassett, Sci. Rep. **6**, 22057 (2016).
[3] A. Zhigalov, G. Arnulfo, L. Nobili, S. Palva, and J. M. Palva, Netw. Neurosci. **1**, 143 (2017).
[4] A. Schnitzler and J. Gross, Nat. Rev. Neurosci. **6**, 285 (2005).
[5] P. Fries, Trends Cogn. Sci. **9**, 474 (2005).
[6] P. Fries, Neuron **88**, 220 (2015).
[7] V. A. Maksimenko, A. Lüttjohann, V. V. Makarov, M. V. Goremyko, A. A. Koronovskii, V. Nedaivozov, A. E. Runnova, G. van Luijtelaar, A. E. Hramov, and S. Boccaletti, Phys. Rev. E **96**, 12316 (2017).
[8] V. A. Maksimenko, A. E. Runnova, N. S. Frolov, V. V. Makarov, V. O. Nedaivozov, A. A. Koronovskii, A. N. Pisarchik, and A. E. Hramov, Phys. Rev. E **97**, 052405 (2018).
[9] V. V. Makarov, M. O. Zhuravlev, A. E. Runnova, P. Protasov, V. A. Maksimenko, N. S. Frolov, A. N. Pisarchik, and A. E. Hramov, Phys. Rev. E **98**, 62413 (2018).
[10] Y. Kuramoto and D. Battogtokh, Nonlin. Phen. Complex Syst. **5**, 380 (2002).
[11] M. J. Panaggio and D. M. Abrams, Nonlinearity **28**, R67 (2015).
[12] L. Larger, B. Penkovsky, and Y. Maistrenko, Nat. Commun. **6**, 7752 (2015).
[13] M. R. Tinsley, S. Nkomo, and K. Showalter, Nat. Phys. **8**, 662 (2012).
[14] E. A. Martens, S. Thutupalli, A. Fourrière, and O. Hallatschek, Proc. Natl. Acad. Sci. USA **110**, 10563 (2013).
[15] T. Kapitaniak, P. Kuzma, J. Wojewoda, K. Czolczynski, and Y. Maistrenko, Sci. Rep. **4**, 6379 (2014).
[16] J. Wojewoda, K. Czolczynski, Y. Maistrenko, and T. Kapitaniak, Sci. Rep. **6**, 34329 (2016).
[17] P. S. Dutta and T. Banerjee, Phys. Rev. E **92**, 042919 (2015).
[18] J. Hizanidis, E. Panagakou, I. Omelchenko, E. Schöll, P. Hövel, and A. Provata, Phys. Rev. E **92**, 12915 (2015).
[19] T. Banerjee, P. S. Dutta, A. Zakharova, and E. Schöll, Phys. Rev. E **94**, 032206 (2016).
[20] J. C. González-Avella, M. G. Cosenza, and M. San Miguel, Physica A **399**, 24 (2014).
[21] M. Wolfrum and O. E. Omel'chenko, Phys. Rev. E **84**, 015201(R) (2011).
[22] S. Boccaletti, A. N. Pisarchik, C. I. del Genio, and A. Amann, *Synchronization: From Coupled Systems to Complex Networks* (Cambridge University Press, Cambridge, 2014).
[23] A. Banerjee and D. Sikder, Phys. Rev. E **98**, 032220 (2018).
[24] S. Majhi, B. K. Bera, D. Ghosh, and M. Perc, Phys. Life Rev. **28**, 100 (2019).
[25] C. R. Laing, Physica D **240**, 1960 (2011).

[26] P. J. Uhlhaas and W. Singer, Neuron **52**, 155 (2006).
[27] P. R. Protachevicz, F. d. S. Borges, E. L. Lameu, K. C. Iarosz, A. H. Kihara, I. L. Caldas, J. D. Szezech, M. S Baptista, E. E. Macau, C. G. Antonopoulos *et al.*, Front. Comput. Neurosci. **13**, 19 (2019).
[28] J. C. Coninck, F. A. Ferrari, A. S. Reis, K. C. Iarosz, A. M. Batista, and R. L. Viana, arXiv:1905.11249.
[29] N. Frolov and A. Hramov, Phys. Life Rev. **28**, 125 (2019).
[30] A. Bandyopadhyay and S. Kar, Appl. Math. Comput. **333**, 194 (2018).
[31] V. A. Maksimenko, V. V. Makarov, B. K. Bera, D. Ghosh, S. K. Dana, M. V. Goremyko, N. S. Frolov, A. A. Koronovskii, and A. E. Hramov, Phys. Rev. E **94**, 52205 (2016).
[32] S. Majhi, M. Perc, and D. Ghosh, Sci. Rep. **6**, 39033 (2016).
[33] N. S. Frolov, V. A. Maksimenko, V. V. Makarov, D. V. Kirsanov, A. E. Hramov, and J. Kurths, Phys. Rev. E **98**, 22320 (2018).
[34] M. Mikhaylenko, L. Ramlow, S. Jalan, and A. Zakharova, Chaos **29**, 023122 (2019).
[35] N. Semenova, A. Zakharova, V. Anishchenko, and E. Schöll, Phys. Rev. Lett. **117**, 014102 (2016).
[36] N. Semenova and A. Zakharova, Chaos **28**, 051104 (2018).
[37] J. Hizanidis, N. E. Kouvaris, G. Zamora-López, A. Díaz-Guilera, and C. G. Antonopoulos, Sci. Rep. **6**, 19845 (2016).
[38] M. S. Santos, J. D. Szezech, F. S. Borges, K. C. Iarosz, I. L. Caldas, A. M. Batista, R. L. Viana, and J. Kurths, Chaos Solitons Fractals **101**, 86 (2017).
[39] T. Chouzouris, I. Omelchenko, A. Zakharova, J. Hlinka, P. Jiruska, and E. Schöll, Chaos **28**, 045112 (2018).
[40] V. V. Makarov, S. Kundu, D. V. Kirsanov, N. S. Frolov, V. A. Maksimenko, D. Ghosh, S. K. Dana, and A. E. Hramov, Commun. Nonlinear Sci. Numer. Simul. **71**, 118 (2019).
[41] B. K. Bera, S. Rakshit, D. Ghosh, and J. Kurths, Chaos **29**, 053115 (2019).
[42] A. N. Pisarchik and U. Feudel, Phys. Rep. **540**, 167 (2014).
[43] D. J. Angeli, E. Ferrell, Jr., and E. D. Sontag, Proc. Natl. Acad. Sci. USA **101**, 1822 (2004).
[44] M. Laurent and N. Kellershohn, Trends Biochem. Sci. **24**, 418 (1999).
[45] J. P. Newman and R. J. Butera, Chaos **20**, 023118 (2010).
[46] B. M. Slepchenko and M. Terasaki, Curr. Opin. Genet. Dev. **14**, 428 (2004).
[47] C. C. Canavier, D. A. Baxter, J. W. Clark, and J. H. Byrne, J. Neurophysiol. **72**, 872 (1994).
[48] A. N. Pisarchik, R. Jaimes-Reátegui, C. D. A. Magallón-García, and C. O. Castillo-Morales, Biol. Cyber. **108**, 397 (2014).
[49] A. E. Hramov, V. A. Maksimenko, S. V. Pchelintseva, A. E. Runnova, V. V. Grubov, V. Y. Musatov, M. O. Zhuravlev, A. A. Koronovskii, and A. N. Pisarchik, Front. Neurosci. **11**, 674 (2017).
[50] A. E. Hramov, M. K. Kurovskaya, A. E. Runnova, M. O. Zhuravlev, V. V. Grubov, A. A. Koronovskii, A. N. Pavlov, and A. N. Pisarchik, in *Proceeding of SPIE, Dynamics and Fluctuations in Biomedical Photonics XIV*, edited by V. V. Tuchin, K. V. Larin, M. J. Leahy, and R. K. Wang, Vol. 10063 (SPIE, 2017), p. 1006314.
[51] J. Hertz, A. Krogh, and R. Palmer, *Introduction to the Theory of Neural Computation* (Addison-Wesley, New York, 1991).
[52] A. E. Runnova, A. E. Hramov, V. V. Grubov, A. A. A. A. Koronovskii, M. K. Kurovskaya, and A. N. Pisarchik, Chaos Solitons Fractals **93**, 201 (2018).
[53] A. N. Pisarchik, P. Chholak, and A. E. Hramov, Chaos Solitons Fractals X **1**, 100005 (2018).
[54] J. Keener and J. Sneyd, *Mathematical Physiology* (Springer, New York, 1998).
[55] D. Shchapin, A. Dmitrichev, and V. Nekorkin, J. Exp. Theor. Phys. Lett. **106**, 617 (2017).
[56] A. S. Dmitrichev, D. S. Shchapin, and V. I. Nekorkin, Front. Appl. Math. Stat. **5**, 9 (2019).
[57] M. Uzuntarla, J. J. Torres, A. Calim, and E. Barreto, Neural Netw. **110**, 131 (2019).
[58] L. M. Mukhametov, A. Y. Supin, and I. G. Polyakova, Brain Res. **134**, 581 (1977).
[59] N. C. Rattenborg, C. J. Amlaner, and S. L. Lima, Neurosci. Biobehav. Rev. **24**, 817 (2000).
[60] P. M. Esir, S. Y. Gordleeva, A. Y. Simonov, A. N. Pisarchik, and V. B. Kazantsev, Phys. Rev. E **98**, 052401 (2018).
[61] A. Hodgkin and A. Huxley, J. Physiol. **117**, 500 (1952).
[62] E. V. Pankratova and A. V. Polovinkin, Eur. Phys. J. B **45**, 391 (2005).
[63] S. Leng, W. Lin, and J. Kurths, Sci. Rep. **6**, 21449 (2016).
[64] S. Rakshit, B. K. Bera, M. Perc, and D. Ghosh, Sci. Rep. **7**, 2412 (2017).
[65] J. A. White, J. T. Rubinstein, and A. R. Kay, Trends Neurosci. **23**, 131 (2000).
[66] D. S. Bassett and E. Bullmore, Neuroscientist **12**, 512 (2006).
[67] V. M. Eguiluz, D. R. Chialvo, G. A. Cecchi, M. Baliki, and A. V. Apkarian, Phys. Rev. Lett. **94**, 018102 (2005).
[68] A.-L. Barabási and R. Albert, Science **286**, 509 (1999).
[69] D. J. Watts and S. H. Strogatz, Nature (London) **393**, 440 (1998).
[70] D. Dudkowski, J. Grabski, J. Wojewoda, P. Perlikowski, Y. Maistrenko, and T. Kapitaniak, Sci. Rep. **6**, 29833 (2016).
[71] I. A. Shepelev, T. E. Vadivasova, A. Bukh, G. Strelkova, and V. Anishchenko, Phys. Lett. A **381**, 1398 (2017).
[72] M. Scheffer, S. R. Carpenter, T. M. Lenton, J. Bascompte, W. Brock, V. Dakos, J. Van de Koppel, I. A. Van de Leemput, S. A. Levin, E. H. Van Nes *et al.*, Science **338**, 344 (2012).